Flow near a Continental Boundary Driven by an Oceanic Jet

HSIEN WANG OU

Lamont-Doherty Earth Observatory, Columbia University, Palisades, New York

(Manuscript received 4 February 1992, in final form 19 August 1993)

ABSTRACT

To provide possible dynamical interpretations of the Gulf Stream–induced circulation in the Middle Atlantic Bight (MAB), the inshore flow driven by a steady and straight jet in a homogeneous ocean is considered via similarity solutions.

To isolate the curvature effect of the coastal boundary, the author first considers the case of a constant-depth ocean, from which various nonlinear flow regimes are discerned. When applied to the MAB, the model can explain the observed intrusion of the Gulf Stream water just downstream of Cape Hatteras where the coastline curves convexly.

Over larger scales of the MAB, the scale analysis suggests the importance of the topography in the vorticity balance. When the topography is included, the similarity solution shows the strong flow to be confined offshore, flanked inshore by a weak counterflow, consistent with the observed slope sea gyre. There is in addition a flow convergence toward the inshore edge of the jet, consistent with the observed occurrence of the shelf water there and the inferred shoreward flux of nutrients across the jet axis.

1. Introduction

Observations show that the Gulf Stream interacts in varied form with the shelf and slope water of the Middle Atlantic Bight (MAB). From current measurements, Csanady and Hamilton (1988) have documented the existence of a cyclonic slope sea gyre with the Gulf Stream forming its offshore boundary, and Bane et al. (1988) have found strong correlation between the shelfbreak current and the position of the Gulf Stream front, suggesting the dynamical linkage of the two. Complementing this gyre circulation, satellite images (e.g., Fig. 19 of Csanady and Hamilton 1988) show an entrainment of the inshore water by the stream, corroborating hydrographic evidence (Ford and Miller 1952).

While these features appear quite persistent, recent studies (Churchill and Cornillon 1991b) suggest, on the other hand, frequent incursions of the Gulf Stream water onto the outer shelf. One episode of such intrusions can be seen in the satellite image (plate 1c of Churchill et al. 1989) that shows a filament of the warm water leaving the Gulf Stream just downstream of Cape Hatteras, turning cyclonically as to direct backward near the shelfbreak.

In the hope of providing dynamical interpretations of these diverse features, I have considered the inshore circulation driven by a steady and straight jet in a homogeneous ocean. Although the dynamics is nonlinear by the implication of a "jet," the vorticity equation nevertheless allows similarity solutions, which greatly simplifies the mathematical task. And despite limitations of such solutions, they provide a powerful tool for depicting possible flow fields and elucidating the underlying dynamical balance.

For the organization of the paper, I shall first discuss in section 2 the model and the use of similarity solutions. Solutions to a constant and variable-depth ocean, as well as their application to the MAB, are then discussed, respectively, in sections 3 and 4. The model results are summarized in section 5.

2. The model

Let us consider a model configuration as shown schematically in Fig. 1, whereby a steady and straight jet interacts with a continental boundary in a homogeneous ocean. Cartesian coordinates are used with the x axis aligned with the jet axis, defined as where the x component of the velocity, u, has a maximum (i.e., $\partial u/\partial y = 0$). The ocean depth is denoted by d, which vanishes at $y = y_b > 0$ marking the coastal boundary. The object of the model is to determine the flow field within the model domain bounded in y by the jet axis and the coastal boundary. For convenience, all the variables are nondimensionalized according to the following scaling rules: Let X be the x scale of interest and Y, U, and D_0 be the values of y, u, and d at (X, 0); then the variables x, y, u, v, and d have been nondimensionalized by X, Y, U, UY/X, and D_0, respectively.

Corresponding author address: Dr. Hsien Wang Ou, Lamont-Doherty Earth Observatory, Columbia University, Palisades, NY 10964.

Since the ocean is homogeneous, the horizontal velocity is depth independent, and the continuity equation can be integrated vertically to yield

$$\nabla \cdot (\mathbf{v}d) = 0, \tag{2.1}$$

which allows the definition of a transport streamfunction ψ as

$$\mathbf{v} = d^{-1}\mathbf{k} \times \nabla\psi. \tag{2.2}$$

As implied by "jet," we neglect the x variation in comparison with the y variation so that the relative vorticity ζ is given by

$$\zeta \equiv \mathbf{k} \cdot \nabla \times \mathbf{v} \approx (d^{-1}\psi_y)_y, \tag{2.3}$$

where the subscripts indicate partial derivatives. We consider a vorticity equation of the form

$$J(\psi, q) = E\zeta_{yy}, \tag{2.4}$$

where J is the Jacobian and $q \equiv d^{-1}(1 + \epsilon\zeta)$ is the potential vorticity. The two dimensionless parameters that have appeared in (2.4) are the Rossby number $\epsilon \equiv U(fY)^{-1}$ with f being the Coriolis parameter, taken to be a positive constant, and the Ekman number $E \equiv \nu X(fY^3)^{-1}$ with ν being the kinematic eddy viscosity. The mathematical task is simply to solve (2.4) in the model domain subject to proper boundary conditions.

Before discussing the boundary conditions, I shall first remark, as to be seen later, that (2.4) can be reduced to an ordinary differential equation by similarity transformations, thus greatly simplifying the task of obtaining a solution (the similarity solution). The well-known trade-off of this simplification is that the similarity solution can satisfy only more restrictive boundary conditions that may limit its application. Along the coastal boundary, the physical condition is that both the normal and tangential components of the velocity vanish, which can be satisfied only if the boundary adheres to certain similarity forms, and obviously the utility of the similarity solution depends on how representative such a boundary is of the boundary of interest.

Similarly, as the x-dependence of the flow is specified by the model geometry through the similarity requirement, the only boundary condition that can be imposed at the jet axis is the scaling definition that u is of unity at (1, 0). That is, the jet is external only in setting the spatial and velocity scales of the inshore flow, which otherwise is governed by the model physics. The implicit assumption is that the jet is forced from offshore so that other properties of the jet, such as its transport, can be accommodated by the spatial dimensions seaward of the jet axis, that is, outside the model domain.

The presence of a forcing region of the jet is obviously required for the overall vorticity balance if the jet were to interact with a coastal boundary since, by virtue of its nonslipness, such a boundary provides a vorticity input that must be removed by forcing. This designation of an offshore forcing region of the jet incidentally stipulates that the unforced balance (2.4) and the ensuing similarity solution may not be extended across the jet axis. The present problem thus differs fundamentally from the channel flows considered in classical fluid mechanics (e.g., see section 5.4 of Batchelor 1970) where the vorticity flux from one boundary can exit through the other boundary so that the inertial-viscous balance (2.4) remains valid throughout the channel. In these latter cases, however, similarity solutions exist only for a symmetric wedge, which is the reason why this is the only geometry that has previously been considered.

While the similarity requirement is restrictive, one mitigating factor sometimes overlooked is that the similarity solution may be applied piecewise in x so long as the edge effect can be neglected. One thus need not be concerned with singularities or the breakdown of the model approximations, such as the narrowness [i.e., Eq. (2.3)] or straightness of the jet, outside the domain of interest that, by scaling definition, encompasses $x = 1$.

To facilitate the similarity solution, let us consider a coastal boundary of the form

$$y_b = x^a, \tag{2.5}$$

where a is an external parameter that may assume either positive or negative value. With the allowance that the jet may be directed forward or backward (with respect to positive x), the form (2.5) is quite general and covers a wide range of model geometries. To isolate the curvature effect of the coastal boundary, I shall first consider the case of a constant-depth ocean.

3. A constant-depth ocean

For a constant-depth ocean, the vorticity equation (2.4) becomes

$$\mathrm{Re}J(\psi, \psi_{yy}) = \psi_{yyyy}, \tag{3.1}$$

where $\mathrm{Re} \equiv \epsilon E^{-1} = UY^2(\nu X)^{-1}$ is the Reynolds number. Since without a variable depth and the ensuing vortex stretching, the fluid does not sense the planetary rotation, (3.1) is the same as that used in the classical nonrotating jet problems (e.g., see chapter 5 of Batchelor 1970), which states the balance between advection and diffusion of vorticity. Although the Reynolds number is typically large for our applications (see section 3d), the inclusion of the viscous term is nevertheless essential since it is of higher order and may singularly perturb the inviscid solution.

To solve (3.1), let us define a new coordinate system (x, η) with (see Fig. 1)

$$\eta \equiv yx^{-a}\epsilon \quad [0, 1], \tag{3.2}$$

and seek a similarity of the form

$$\psi = x^b\phi(\eta), \tag{3.3}$$

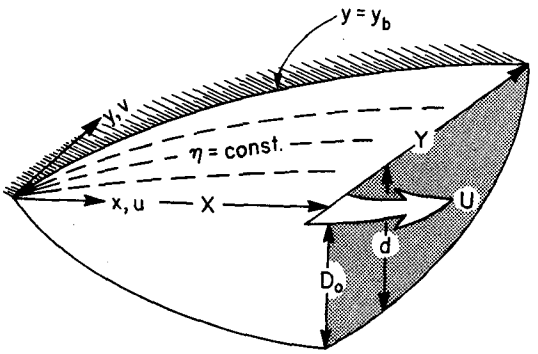

FIG. 1. A schematic of the model configuration that defines some symbols used in the model.

where b is a constant yet to be determined. Substituting (3.3) into (3.1), and requiring the equation to hold over a finite range of x, yields

$$b = 1 - a, \tag{3.4}$$

or, as alluded to in the previous section, the x dependence of the flow is determined by the model geometry. In particular, $a = 1$ (a divergent wedge) marks the transition from increasing to decreasing transport with x, and since

$$u = -\psi_y = -x^{1-2a}\phi'(\eta), \tag{3.5}$$

the value $a = 1/2$ marks the transition from increasing to decreasing u with x. In terms of the similarity variable ϕ, (3.1) becomes

$$\mathrm{Re}[(1 - a)\phi\phi''' - (1 - 3a)\phi'\phi''] = \phi'''', \tag{3.6}$$

where the two terms on the left-hand side represent the advection of vorticity across and along constant-η lines, referred to henceforth as "spanwise" and "streamwise," respectively, which are balanced by the diffusion of vorticity on the right-hand side.

The boundary conditions, as stated earlier, become, for a forward jet,

$$\phi(1) = \phi'(1) = 0, \quad \phi'(0) = -1$$
$$\text{and} \quad \phi''(0) = 0 (\phi'''(0) > 0). \tag{3.7}$$

That is, the coastal boundary is nonporous and nonslip, and u has a maximum along the jet axis (by definition) with a unit magnitude at (1, 0) (by scaling). For a backward jet, the signs in (3.7) are reversed, but since (3.6) is invariant to the transformation $\phi \to -\phi$, Re $\to$ −Re, the backward jet case can be accommodated by the same equations (3.6) and (3.7) but with a negative Re.

As alluded to before, the mathematical problem is reduced to that of solving an ordinary differential equation (3.6), the numerical method of which is described in the Appendix. As the solution depends only on the parameter a characterizing the boundary shape, and the Reynolds number Re, the flow property can be fully explored on the parameter plane of (a, Re), with both parameters assuming positive as well as negative values. To facilitate the discussion, I shall first consider the linear solution (Re = 0), then its modification by the advective terms ($|\mathrm{Re}| \ll 1$), and then the strongly nonlinear solution ($|\mathrm{Re}| \gg 1$) which are more pertinent for the present problem.

a. The linear regime (Re = 0)

Setting Re = 0 in (3.6), the equation becomes

$$\phi'''' = 0, \tag{3.8}$$

or there is a uniform diffusive flux of vorticity transversing the model domain. The solution is given by

$$\phi = \frac{1}{3}(\eta^3 - 1) - (\eta - 1), \tag{3.9}$$

and the corresponding u at $x = 1$ [i.e., $-\phi'$ from Eq. (3.5)] for a forward jet is plotted (the solid line) in Fig. 2. Since the linear balance involves only spanwise derivatives, this velocity profile is independent of the boundary geometry; the jet is thus broad with increasing shear toward the coastal boundary. The x dependence of the streamfunction (and hence the transverse flow) is however a function of the model geometry as given by (3.3) and (3.4), and the flow exactly reverses for a backward jet.

b. The weakly nonlinear regime ($|Re| \ll 1$)

Since the advective term in (3.6) is of lower order than the viscous term, they only regularly perturb the linear solution. One may thus expand the solution in

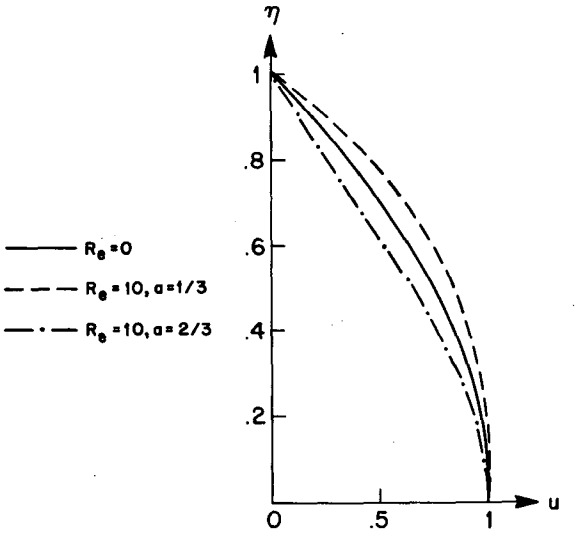

FIG. 2. The profile of u at $x = 1$ of a constant-depth ocean for the linear regime of Re = 0 (the solid line), and the weakly nonlinear regimes of Re = 10, $a = 1/3$ (the dashed line) and Re = 10, $a = 2/3$ (the dash-dotted line).

perturbation series in Re, uniformly valid in η, and then derive the expression for the perturbations. While such exercises show that the advective term may vary in sign in the model domain, its net effect on the vorticity balance of a (spanwise) strip of fluid, however, is more definitive and may be used to infer the modification of the linear solution. Integrating (3.6) from $\eta = 0$ to 1 yields

$$\mathrm{Re}(1 - 2a) = [\phi''']_0^1. \tag{3.10}$$

So for an accelerating jet when $\mathrm{Re}(1 - 2a) > 0$ [recalling Eq. (3.5) and taking into account the sign of Re], there is an enhanced diffusive flux of vorticity from the coastal boundary relative to that exiting the jet axis, and for a decelerating jet, the opposite is true. This modification of the linear solution is clearly demonstrated by the numerical solutions shown in Fig. 2.

To understand this result, one notes that since the spanwise vorticity flux vanishes at the coastal boundary (because of zero normal velocity) and the jet axis (because of zero relative vorticity), the net advection depends on the x variation of the streamwise vorticity transport, which is directly related to the jet speed via

$$\int_0^{y_b} u\zeta dy = -\int_0^{y_b} uu_y dy = \frac{1}{2}u(0)^2. \tag{3.11}$$

So for an accelerating jet, for example, one has a divergence of this vorticity transport, which must be balanced by a net diffusive input or a sharpening of the vorticity gradient at the coastal boundary relative to that at the jet axis, as deduced above.

One, however, may not extrapolate from above modification of the linear solution to infer that the viscous effect will be increasingly confined to the respective boundary as Re increases, since such an inference presumes the existence of an inviscid interior, which, as we shall see below, may not be attainable, and viscosity may remain important throughout the model domain even as $\mathrm{Re} \to \infty$.

c. *The strongly nonlinear regime ($|\mathrm{Re}| \gg 1$)*

The approach adopted here is to first presuppose the existence of an inviscid interior and then inquire whether a viscous boundary layer can be appended to satisfy all the boundary conditions. If the answer is affirmative, one hopes the derivation of the solution would ensure its uniqueness. If, on the other hand, the answer is negative, one has to accept the falsehood of the above presumption and conclude that the viscous effect remains important throughout the model domain. This latter possibility of course stems from the singular nature of the viscous term, which may dominate the balance given sufficiently small scales (i.e., the flow undulates sufficiently rapidly in η) even as Re becomes large.

In the inviscid interior (and hence the subscript I), the solution satisfies the equation

$$(1 - a)\phi_I\phi_I''' - (1 - 3a)\phi_I'\phi_I'' = 0, \tag{3.12}$$

which is of the third order and, in general, can satisfy only three boundary conditions, with the higher-order condition of (3.7) at either boundary remaining unsatisfied. The two cases will be labeled as case "0" and "1," corresponding to the "value of η" where the boundary conditions are not fully satisfied by the inviscid flow and where there is a possible viscous boundary layer.

For case 1 with the nonslip condition at $\eta = 1$ relaxed, (3.12) can be integrated once to yield

$$(1 - a)\phi_I\phi_I'' - (1 - 2a)(\phi_I'^2 - 1) = 0, \tag{3.13}$$

which has a trivial solution

$$\phi_I = 1 - \eta, \tag{3.14}$$

and the corresponding u is uniform in η.

To show that this is a unique solution, let us assume the existence of nontrivial solutions so that (3.13) may be multiplied by $\phi_I'\phi_I^{-1}(\phi_I'^2 - 1)^{-1}$ and integrated once to yield

$$\phi_I' = \mp[1 + A\phi_I^{2(1-2a)/(1-a)}]^{1/2}, \tag{3.15}$$

where A is an unknown constant. Because of the square root appearing on the rhs, ϕ_I' can be of only one sign through the model domain, and hence the boundary condition $\phi_I(1) = 0$ necessarily implies $\phi_I(0) \neq 0$. To satisfy the boundary condition $\phi_I'(0) = -1$, one then requires $A = 0$ and the negative sign be chosen in (3.15). One thus has $\phi_I' = -1$ identically, contradicting the nontrivialness of such solutions.

To assess whether the nonslip condition at $\eta = 1$ can be satisfied by appending a viscous boundary layer, one integrates the full equation (3.6) across such a boundary layer and uses the interior solution (3.14) to yield

$$\mathrm{Re}(1 - 2a) \approx \phi'''(1). \tag{3.16}$$

Since to adjust a positive u in the interior to zero at the boundary implies $\phi'''(1) > 0$, the balance is possible only if $\mathrm{Re}(1 - 2a) > 0$ or the flow is accelerating downstream, a result well known in classical fluid dynamics (see section 5.9 of Batchelor 1970). The physical reason is a trivial extension of that offered in section 3b; namely, only an accelerating flow in the interior can provide a divergence of vorticity flux to the viscous boundary layer, necessary to remove the diffusion of vorticity from the coastal boundary. For an accelerating jet, the solution thus behaves regularly as Re increases, with the viscous boundary layer increasingly pressed against the coastal boundary. The width of this boundary layer can be seen from (3.16) to be scaled as $\mathrm{Re}^{-1/2}$ since ϕ' varies through a unit magnitude across the boundary layer. The numerical solution for the case of $\mathrm{Re} = 50$, $a = 1/3$ is plotted in Fig. 3, which exhibits the above structure.

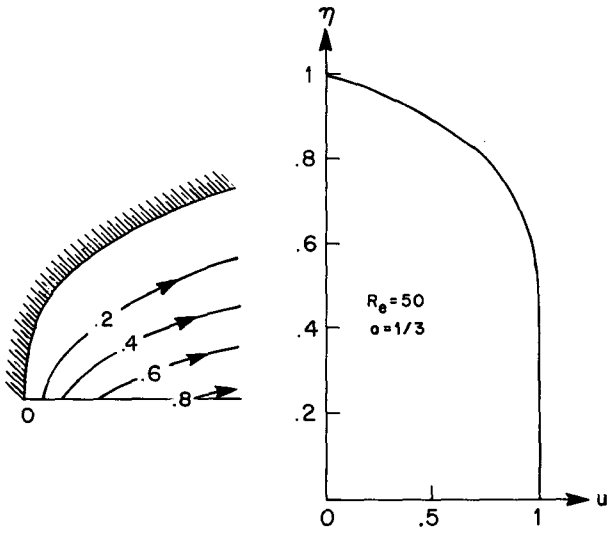

FIG. 3. Same as Fig. 2 but for the strongly nonlinear regime of Re = 50, a = 1/3. The coastal geometry and the streamlines are also plotted. The advection has expelled the viscous effect to the coastal boundary where there is a strong shear layer.

For case 0, when the zero vorticity condition at $\eta = 0$ is relaxed for the inviscid flow, (3.12) can be integrated repeatedly to yield

$$\phi_I = a(1-a)^{-1}(1-\eta)^{(1-a)/a}, \qquad (3.17)$$

with the requirement that

$$0 < a < \frac{1}{2}. \qquad (3.18)$$

It is trivial to see that outside this parameter range the solution (3.17) cannot satisfy the two coastal boundary conditions and hence there is no solution.

To examine whether a viscous boundary layer can be appended at $\eta = 0$ to satisfy the relaxed boundary condition that $\phi''(0) = 0$, we again integrate the full equation (3.6) across such a boundary layer and use (3.17) to obtain

$$\mathrm{Re}a\phi_I''(0) \approx -\phi'''(0), \qquad (3.19)$$

which states the balance between the advective (in the spanwise direction) and diffusive flux of vorticity. Since $\phi''(0) = 0$, $\phi'''(0)$ is of the same sign as $\phi_I''(0)$, the balance is possible only if Re < 0, or the jet is directed backward. Physically, this is because in the parameter range of (3.18), the transport increases with x [Eqs. (3.3) and (3.4)]; hence, only a backward jet is accompanied by an offshore flow that can balance the diffusive flux of vorticity across the jet axis.

For a more formal derivation, one can decompose the solution as the sum of the interior solution (3.17) and a boundary-layer correction ϕ_B:

$$\phi = \phi_I + |\mathrm{Re}|^{-2}\phi_B(\xi), \qquad (3.20)$$

with $\xi(\equiv|\mathrm{Re}|^{-1}\eta)$ being the stretched coordinate. Substituting (3.20) into (3.6), ϕ_B satisfies the linear equation

$$\pm a\phi_{B\xi\xi\xi} = \phi_{B\xi\xi\xi\xi}, \qquad (3.21)$$

and the boundary conditions $\phi_{B\xi\xi}(0) = -\phi_I''(0)$, and $\phi_B \to 0$ as $\xi \to \infty$. The two signs in (3.21) correspond to the sign of Re, hence and as expected, a solution is possible only if Re is negative. A numerical solution for the case of a = 1/3, Re = −50 is plotted in Fig. 4, which exhibits the deduced flow structure. Since the boundary layer has a width scaled by $|\mathrm{Re}|^{-1}$, it is much narrower than that of case 1, and it is characterized by large vorticity gradient rather than large shear. But despite these differences, u is of a single sign for both cases with no counterflows in the interior.

By way of above analysis, we have exhausted the parameter ranges for which there is an inviscid interior; namely, $\mathrm{Re}(1-2a) > 0$ for case 1 and Re < 0, $0 < a < 1/2$ for case 0. Outside these parameter ranges, the viscous effect should be important throughout the model domain by the generation of undulating flows, a numerical example of which is plotted in Fig. 5 for the case of Re = 10, a = 2. Using (3.10), one can crudely estimate the spanwise scale δ as

$$\delta \approx \mathrm{O}[|\mathrm{Re}(1-2a)|^{-1/2}], \qquad (3.22)$$

which expectedly decreases as |Re| increases or as the model geometry becomes more divergent. One may further estimate the critical Reynolds number $|R_n|$ for the onset of the nth oscillatory mode (i.e., with n zero crossings in u inside the model domain). Since such onsets coincide with a vanishing shear at the coastal boundary, and recalling that current shear also

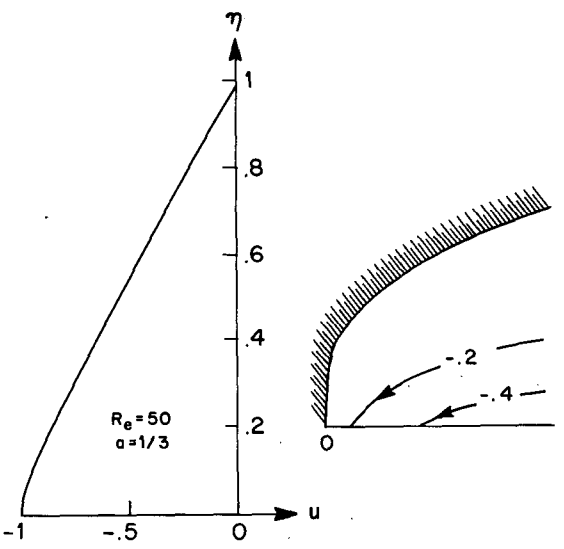

FIG. 4. Same as Fig. 3 but for a backward jet of Re = −50, a = 1/3. The advection has expelled the viscous boundary layer to the jet axis where there is a large vorticity gradient.

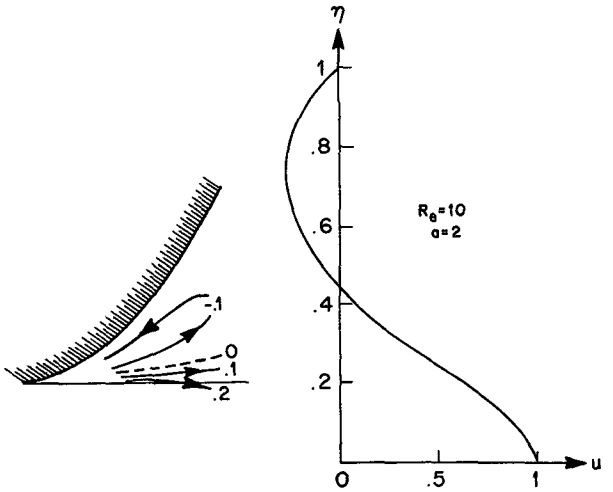

FIG. 5. Same as Fig. 3 but for the case of Re = 10, a = 2. The viscous effect is important throughout the model domain due to its generation of undulating flows.

vanishes at the jet axis, the model domain should contain n half-cycles, or

$$\delta \approx O([n\pi]^{-1}). \tag{3.23}$$

Combining (3.22) and (3.23), one derives

$$|R_n| \approx O[n^2\pi^2|1-2a|^{-1}]. \tag{3.24}$$

We have plotted the expression within the above bracket for the first mode (n = 1) in Fig. 6 (the dashed lines), the order of magnitude of which encompasses the numerical values shown as vertical bars. For a = 1, incidentally, our numerical value agrees with Batchelor's (1970) value of 10.31 [his Eq. (5.6.15)], affirming the accuracy of our numerical calculations. Since $|R_n|$ varies as n^2, the prospect of generating higher modes is rapidly diminishing with the mode number.

Since the fluid in the counterflow inshore of the jet may either be entrained into or detrained from the jet, depending on the coastline geometry [Eqs. (3.3) and (3.4)], one can discern four distinctive nonlinear flow regimes as indicated in Fig. 6 (separated by hatched lines and labeled by Roman numerals). In Regime I [Re$(1-2a)>0$], the jet accelerates downstream. The strong flow extends through the inviscid interior to the coastal boundary where a viscous shear layer is confined. In Regime II (Re <0, $0<a<1/2$), the jet decelerates downstream in a convergent geometry. There is also an inviscid interior where the flow has an offshore component that expels the viscous boundary layer to the jet axis characterized by a large vorticity gradient. In Regime III (Re >0, $1/2<a<1$), the jet decelerates in a divergent and concave (seaward) geometry. Viscosity is important throughout the model domain by the generation of undulating flows (only the schematic for the first mode is shown). The jet entrains fluid from both the adjacent counterflow and

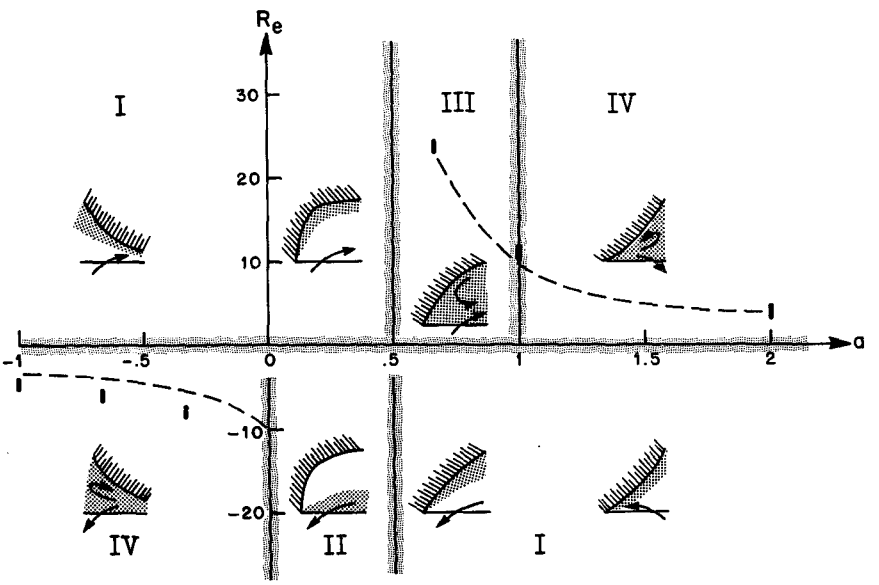

FIG. 6. A diagram showing the nonlinear flow regimes of a constant-depth ocean on the parameter plane of a, characterizing the boundary shape, and the Reynolds number Re. Different regimes are separated by shaded bands and labeled by Roman numerals, and the associated flow directions are indicated by arrows (only the first mode is shown for undulating flows). The dotted regions indicate where the viscous effect is important. The dashed lines are the order of magnitude estimates of the critical Rossby number for the onset of the first undulating mode [from Eq. (3.24)], and short vertical bars are its values determined from numerical calculations.

across the jet axis, which converges at the cyclonic flank of the jet. In Regime IV (Re $>$ 0, $a > 1$ and Re $<$ 0, $a < 0$), the jet decelerates in a divergent and convex (seaward) geometry. The flow is again undulating and viscous throughout the model domain, but the water in the jet is detrained into the counterflow and across the jet axis.

d. Applications

While the topography may be important in explaining the flow in the MAB (see section 4), it nevertheless is useful to infer the flow structure from a constant-depth model to assess the curvature effect of the coastal boundary and to reveal possible shortfalls of such a model. For obvious reasons, the coastal boundary of a constant-depth model should be identified with the shelfbreak, along which the boundary conditions of vanishing normal and tangential velocities can be justified by the shallowness of the shelf and the enhanced bottom drag that prohibit strong flows.

One notes from the topography map shown in Fig. 7 that the coastal boundary assumes different similarity forms depending on the x scale of interest. Over the smaller scale immediately downstream of Cape Hatteras, the coastal boundary curves convexly (seaward), but over the larger scale of the MAB, the coastal boundary is concave. Superimposed on Fig. 7 are some model approximations based on the observed mean position of the Gulf Stream front [the hatched line, taken from Halliwell and Mooers (1979)]. Specifically, we have used $X = 100$ km, $Y = 100$ km, and $a = 2$ for the small-scale case, and $X = 600$ km, $Y = 300$ km, and $a = 1/3$ and $2/3$ for the larger-scale case. If one uses in addition $U = 3$ m s^{-1}, $f = 10^{-4}$ s^{-1}, and $\nu = 5 \times 10^{7}$ cm s^{-2}, one estimates that $(\epsilon, E) = (3 \times 10^{-1}, 5 \times 10^{-3})$, and $(10^{-1}, 10^{-3})$ for the small- and large-scale case, respectively, and the corresponding Reynolds number is 60 and 100. While these estimates are highly uncertain, they are only used to infer possible flow regimes.

Judging from Fig. 6, the small-scale case ($a = 2$, Re $= 60$) would fall in Regime IV, or there should be a detrainment of the Gulf Stream water into a counterflow inshore of the stream. The model flow thus resembles the observed Gulf Stream intrusions described in section 2. For the large-scale case, the uncertainty of the geometric parameter a allows the possibility of two distinctively different flow regimes I and III. While the latter is consistent with the observation of a Gulf Stream entraining fluid from an inshore counterflow, the former, however, shows a Gulf Stream extending to the shelfbreak, clearly at variance with observations. Because of the smaller Rossby number in the large-scale case, one expects an enhanced topographic effect in the vorticity balance. Does the inclusion of topography qualitatively change the solution so as to remove the above ambiguities and improve the model comparison with observations? To answer this question, we shall next consider an ocean of variable depth.

4. A variable-depth ocean

One can see from the vorticity equation (2.4) that the importance of the vortex stretching is measured by the axial topographic slope (normalized by D_0X^{-1}) at (1, 0). Based on Fig. 3 of Watts (1983), we use a physical slope of 4×10^{-3} and D_0 of 2 and 4 km, respectively, for the small- and large-scale case; then the corresponding normalized slope has a value of 0.2 and 0.6. With the respective Rossby number estimated in the previous section to be 0.3 and 0.1, the topographic stretching would dominate the advective effect in the large-scale case. Since the vortex stretching as the jet enters the deeper water tends to increase the cyclonic shear, opposite the advective effect of an accelerating jet in a constant-depth ocean (section 3b), one foresees the possibility that the flow in Regime I could be qualitatively altered by a finite topographic slope.

To facilitate the similarity solution, one considers a depth of the form

$$d = x^c D(\eta), \tag{4.1}$$

where η is the similarity coordinate defined in (3.2), c is an external parameter characterizing the axial slope of the topography, and D specifies the transversal depth profile. Since isobaths are generally oriented as the coastal boundary, c is taken to be positive, so that the jet enters the deeper water in a divergent geometry.

Seeking a similarity solution to (2.4) of the form

$$\psi = x^{b+c}\phi(\eta), \tag{4.2}$$

one derives, in addition to (3.4), that

$$a = \frac{1}{3}. \tag{4.3}$$

The inclusion of a finite topographic slope thus further constrains the allowable model geometry for similarity solutions. But since $a = 1/3$ can be representative of the large-scale geometry of the MAB (Fig. 7) and since it is this geometry that the constant-depth solution is the most at variance with observations and needs rectification, one may still address the question posed at the end of the last section. Furthermore, as we shall see later, a finite topography tends to insulate the jet from the coastal boundary and hence reduce the flow dependence on the specific form of such boundaries.

For later references, one notes that for this model geometry,

$$u = -d^{-1}\psi_y = -x^{1/3}\phi'/D, \tag{4.4}$$

the magnitude of which increases with x, and

$$\zeta = -u_y = (\phi'/D)', \tag{4.5}$$

which is constant in x. In terms of the similarity variables, the vorticity equation (2.4) becomes

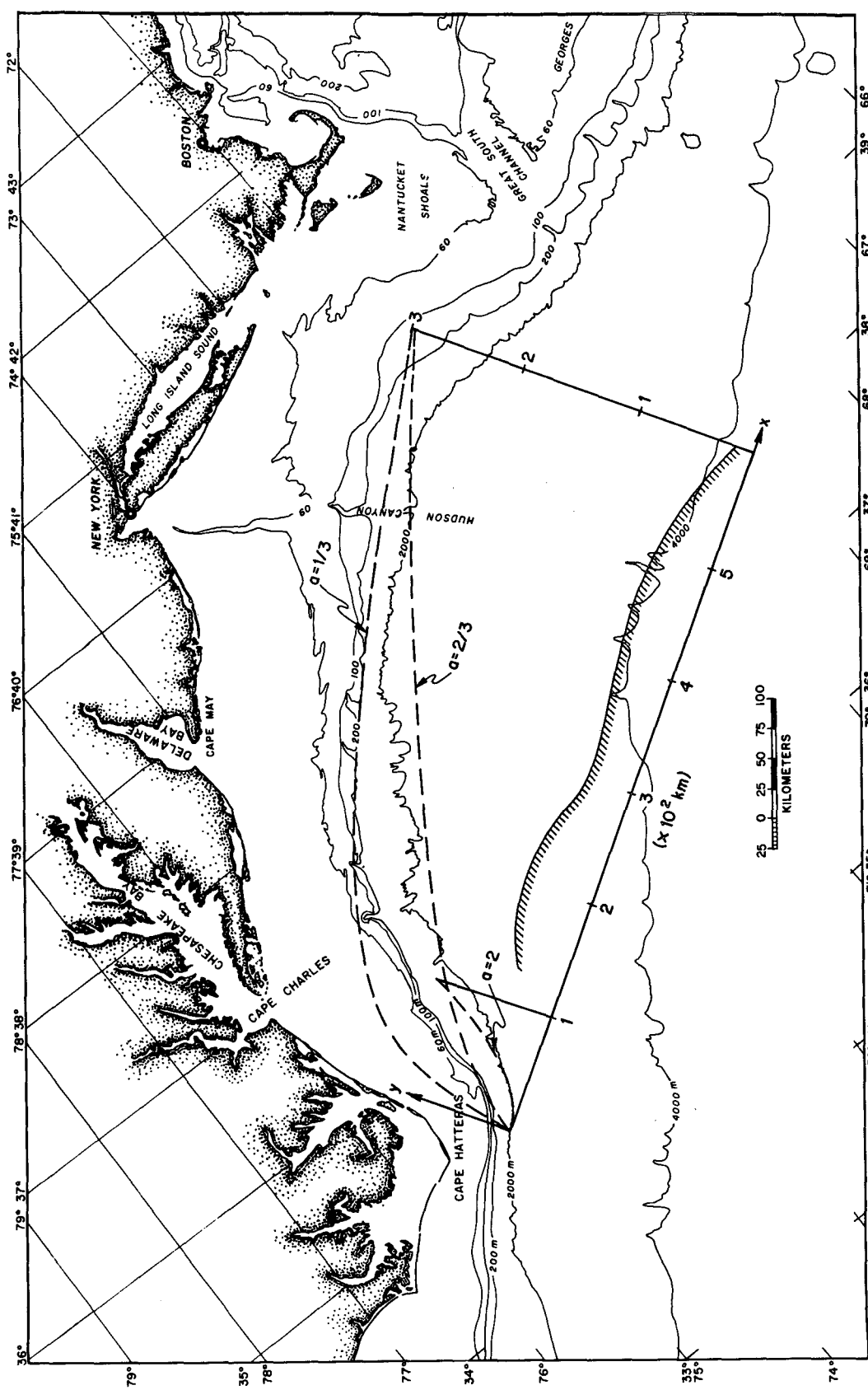

FIG. 7. Model approximations of the MAB. The hatched curve is the mean position of the Gulf Stream front taken from the Halliwell and Mooers (1979). For the smaller scale in the vicinity of the Cape Hatteras, $X = 100$ km, $Y = 100$ km, and $a = 2$. And for the larger scale of the MAB as a whole, $X = 600$ km, $Y = 300$ km, and two values of a (⅓ and ⅔) are used.

$$\left(\frac{2}{3}+c\right)\phi Q' + c\phi' Q = E(\phi'/D)''', \tag{4.6}$$

where $Q \equiv D^{-1}[1 + \epsilon(\phi'/D)']$ is the potential vorticity. The two terms on the lhs represent, respectively, the span- and streamwise advection of potential vorticity, which is balanced on the rhs by the diffusion of vorticity. Equation (4.6) can also be written as

$$\underbrace{\left[1+\epsilon\left(\frac{\phi'}{D}\right)'\right]\left[\left(\frac{2}{3}+c\right)\phi\left(\frac{1}{D}\right)' + c\frac{\phi'}{D}\right]}_{\text{STR}} + \underbrace{\epsilon\left(\frac{2}{3}+c\right)\frac{\phi'}{D}\left(\frac{\phi'}{D}\right)''}_{\text{ADV}} = \underbrace{E\left(\frac{\phi'}{D}\right)'''}_{\text{VIS}}, \tag{4.7}$$

where the advection of potential vorticity is separated into vortex stretching (the term marked STR) and the spanwise advection of relative vorticity (the term marked ADV)—recall from (4.5) that the relative vorticity is constant in x so that its streamwise advection vanishes. The viscous term is marked VIS. Based on the earlier estimates of ϵ, E, and c for the large-scale case, we shall only be concerned with the parameter range of

$$\epsilon, E \ll c \leqslant O(1). \tag{4.8}$$

Taking into account of the variable depth, the boundary conditions (3.7) are slightly modified to

$$\phi(1) = \frac{\phi'}{D}(1) = 0, \quad \frac{\phi'}{D}(0) = -1 \quad \text{and}$$
$$\left(\frac{\phi'}{D}\right)'(0) = 0\left[\left(\frac{\phi'}{D}\right)''(0) > 0\right]. \tag{4.9}$$

To facilitate the following discussion, we shall first consider the linear and then the strongly nonlinear solutions.

a. The linear regime ($\epsilon = 0$)

Setting ϵ to zero in (4.7), we have the linear equation

$$\left(\frac{2}{3}+c\right)\phi\left(\frac{1}{D}\right)' + c\frac{\phi'}{D} = E\left(\frac{\phi'}{D}\right)'''. \tag{4.10}$$

Since $E \ll 1$, one can expand the solution in the interior as

$$\phi_I = \sum_{n=0}^{\infty} E^n \phi_n. \tag{4.11}$$

Substituting (4.11) into (4.10), one derives that

$$\phi_0 = A_0 D^p, \tag{4.12}$$

and

$$\phi_n = c^{-1} D^p \int D^{1-p}\left(\frac{\phi'_{n-1}}{D}\right)''' d\eta \quad (n = 1, 2, \cdots), \tag{4.13}$$

where $p \equiv 1 + 2/(3c)$, and A_0 is an unknown constant. Depending on the depth profile $D(\eta)$ and the value of p, the series may either terminate after finite terms or the higher-order terms are singular at $\eta = 1$ where the depth vanishes. To satisfy the homogeneous boundary conditions at $\eta = 1$, there is a trivial solution of $A_0 = 0$ corresponding to a motionless interior. Indeed, as we shall argue below that since there cannot be a viscous boundary layer at $\eta = 1$, this is likely to be the only solution except for some specialized topography when the interior solution (4.11) satisfies by itself the coastal boundary conditions.

To advance this argument, let us suppose there is a viscous boundary layer at $\eta = 1$, and express the boundary-layer solution as the sum of the interior solution and a boundary-layer correction

$$\phi = \phi_I + \phi_B(\xi), \tag{4.14}$$

where $\xi\ (\equiv \delta^{-1}[1 - \eta])$ is a stretched coordinate with δ being a small parameter to be determined below. For convenience, we assume $D'(1) \neq 0$, although the following derivation is not significantly altered otherwise. Substituting (4.14) into (4.10), one deduces that $\delta = E^{1/3}$ and ϕ_B satisfy the equation

$$\left(\frac{2}{3}+c\right)\phi_B\xi^{-2} - c\phi_{B\xi}\xi^{-1} = (\phi_{B\xi}\xi^{-1})_{\xi\xi\xi}. \tag{4.15}$$

Since in the matching region ($\xi \to \infty$, $1 - \eta \to 0$) the approximate balance is

$$-c\phi_{B\xi} \approx \phi_{B\xi\xi\xi\xi}, \tag{4.16}$$

it allows only one decaying solution, not sufficient to satisfy both boundary conditions at $\eta = 1$. We infer then that there cannot be a viscous boundary layer at $\eta = 1$ and the only permissible interior solutions are the ones that satisfy by themselves the coastal boundary conditions at $\eta = 1$. As an example, for a bottom sloping uniformly in η (i.e., $D' = -1$), it is straightforward to see that the degenerate case (i.e., there exist nontrivial solutions) requires p to be an integer other than $2 + 3n$ ($n = 0, 1, \cdots$).

The validity of the interior solution also depends on whether the two boundary conditions at $\eta = 0$ can be satisfied by appending a viscous boundary layer. To examine this, we again expand the boundary-layer solution as in (4.14), but with the stretched coordinate ξ now defined as $E^{-1/3}\eta$, the boundary correction ϕ_B then satisfies, to the lowest order,

$$c\phi_{B\xi} \approx \phi_{B\xi\xi\xi\xi}, \tag{4.17}$$

which allows two decaying solutions, and hence, both boundary conditions at $\eta = 0$ can be satisfied regardless of the interior solution. We have thus deduced through asymptotic analysis that either A_0 is arbitrary for a degenerate case requiring specialized topography or $A_0 = 0$ otherwise. Since the nontrivial solution is more susceptible to modification by changing topography or

addition of other physics such as the advection to be included later, one expects the trivial solution to be of more practical importance. Furthermore, since E is not infinitesimal, one can only conclude that $A_0 \ll 1$ in the trivial case, or the interior flow is severely constrained by a finite topographic slope. The strong flow is thus confined to an offshore viscous boundary layer next to the jet axis where the vortex stretching is balanced by the lateral diffusion of vorticity [Eq. (4.17)].

A linear solution for the forward jet is plotted in Fig. 8, which is seen to contrast sharply with the corresponding solution in a constant-depth ocean (Fig. 2). Instead of a broad flow of increasing shear toward the coastal boundary, the velocity component u undulates as it decays shoreward. Since the net transport is directed forward and, according to (4.2), increases downstream, there is a shoreward flow crossing the jet axis. It is worth noting that since the boundary-layer width is scaled by $E^{1/3}$, even for this example of $E = 10^{-3}$, the forward flow extends quite deeply into the interior.

b. *The strongly nonlinear regime ($\epsilon \gg E^{1/3}$)*

Since, as seen above, the linear flow has a shoreward component at the jet axis where the relative vorticity is zero, the incorporation of advection tends to reduce the local shear and broaden the jet. But as the advective terms are of lower order than the viscous term, they do not substantially alter the argument put forth in the previous section regarding the absence of a boundary layer at $\eta = 1$, the interior flow thus remains severely constrained by topography. That is, to the lowest order,

$$\phi_I = A_0 D^p, \tag{4.18}$$

with

$$A_0 \leqslant O(\epsilon, E) \ll 1. \tag{4.19}$$

Thus, in contrast to the constant-depth case when the strong flow extends to the coastal boundary by the advection, the finite topographic slope confines the strong flow to an offshore boundary layer next to the jet axis.

To elucidate the dynamical balance of this boundary layer, one expands the boundary-layer solution as

$$\phi = \phi_I(\eta) + \delta\phi_B(\xi), \tag{4.20}$$

where $\xi(\equiv \delta^{-1}\eta)$ is the stretched coordinate with δ being a small parameter yet to be determined. The boundary-layer correction is of $O(\delta)$ due to the condition that u is of unit magnitude at $\eta = 0$. Substituting (4.20) into (4.7) yields, to the lowest order,

$$\underbrace{(1 + \epsilon\delta^{-1}\phi_{B\xi\xi})\, c\phi_{B\xi}}_{\text{STR}} + \underbrace{\epsilon\delta^{-1}\left(\frac{2}{3} + c\right)(\delta^{-1}A_0 + \phi_B)\phi_{B\xi\xi\xi}}_{\text{ADV}} \approx \underbrace{E\delta^{-3}\phi_{B\xi\xi\xi\xi}}_{\text{VIS}}. \tag{4.21}$$

If one balances the stretching with the viscous term, one obtains a viscous boundary-layer width of $\delta = E^{1/3}$. If, on the other hand, one balances the stretching with the advective term and recalls (4.19), one obtains an inertial boundary-layer width of $\delta = \epsilon$. So the nature of the boundary layer depends on the relative magnitude of $E^{1/3}$ and ϵ. The linear regime discussed in the previous section corresponds to the case $\epsilon \ll E^{1/3}$, and for the nonlinear regime considered here, $\epsilon \ll E^{1/3}$, (4.21) becomes

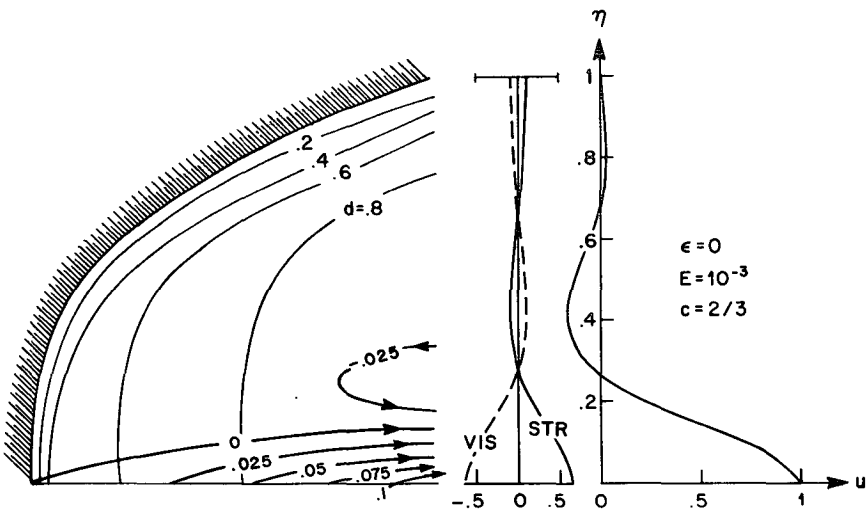

FIG. 8. Same as Fig. 3 but for a variable-depth ocean and for the linear regime of $\epsilon = 0$, $E = 10^{-3}$, $c = 2/3$ and a depth profile of $D(\eta) = \tanh(5[1 - \eta])/\tanh(5)$ (the corresponding isobaths are plotted in thin solid lines). The magnitude of the terms in the vorticity balance (4.7) are also plotted (the advective term is zero for the linear regime).

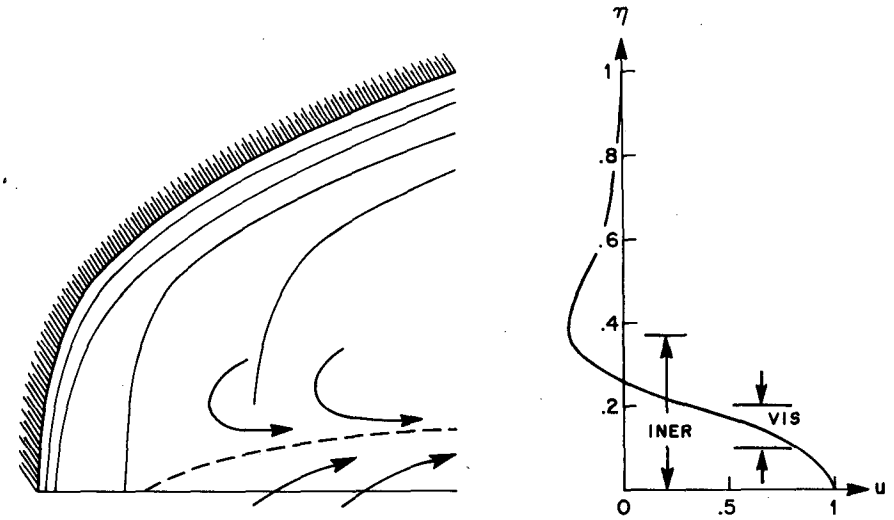

FIG. 9. A schematic for the strongly nonlinear flow in a variable-depth ocean. The jet is confined to an offshore inertial boundary layer where the vortex stretching as the jet enters the deeper water is balanced by flow convergence toward the maximum cyclonic shear (the dashed line) where an inner viscous boundary layer is confined. The entrainment of the inshore water by the jet induces a weak and broad counterflow in the interior.

$$(1 + \phi_{B\xi\xi})c\phi_{B\xi} + \left(\frac{2}{3} + c\right) \times (\epsilon^{-1}A_0 + \phi_B)\phi_{B\xi\xi\xi} \approx E\epsilon^{-3}\phi_{B\xi\xi\xi\xi\xi}\,, \quad (4.22)$$

so there will be an outer inertial boundary layer encompassing an inner viscous boundary layer.

To see how the presence of the inertial boundary layer constrains the interior flow, one notes from (4.22) that in the matching region to the interior where the boundary-layer correction is small, it satisfies the approximate equation

$$c\phi_{B\xi} + \left(\frac{2}{3} + c\right)\epsilon^{-1}A_0\phi_{B\xi\xi\xi} \approx 0\,, \quad (4.23)$$

which has a decaying solution only if A_0 is negative, or the interior flow is directed backward and entrained into the jet. One should point out that this entrainment is quite different from that of a classical jet caused by conservation of the momentum flux (section 5.12 of Batchelor 1970; Rossby 1936). The present entrainment is caused by the vortex stretching that requires a convergence of low vorticity water at the cyclonic side of the jet.

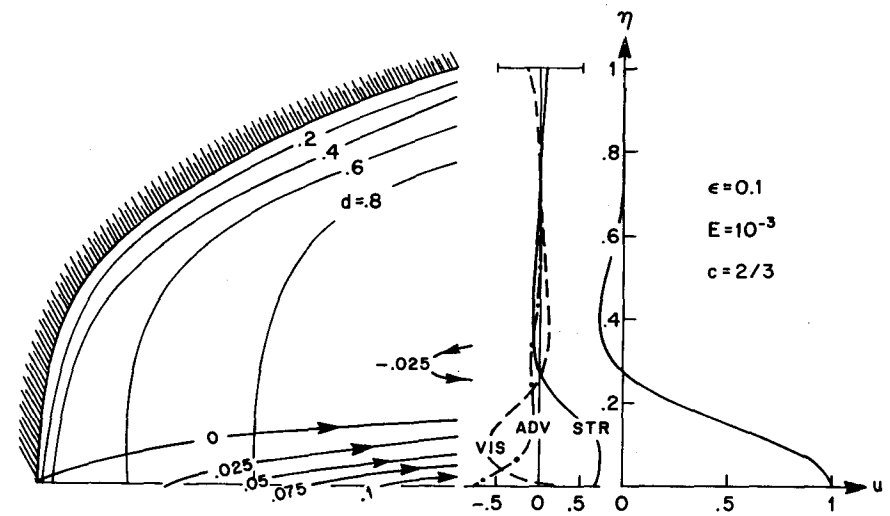

FIG. 10. Same as Fig. 8 but for $\epsilon = 0.1$. From the vorticity balance, one observes the displacement of the viscous boundary layer to the cyclonic flank of the jet, as suggested by the schematic of Fig. 9.

For the inner viscous boundary layer, there appears to be two possible configurations, depending on whether the streamfunction [$\epsilon^{-1}A_0 + \phi_B$ in Eq. (4.22)] vanishes within the inertial boundary layer, or equivalently, whether the net transport is directed forward within the model domain. If this is the case, the viscous boundary layer is confined to the line of flow convergence, which must also align with the maximum cyclonic shear because of the inviscid balance outside this boundary layer; that is, the vortex stretching is balanced by the convergence of low-vorticity water. If, on the other hand, the transport in the counterflow cannot be fully absorbed by the forward flow within the model domain, there would be an offshore flow across the jet axis where the viscous boundary layer is expelled. But since this case requires a greater interior transport, it implies some degeneracy in the interior and, for the same reason given in section 4.c, is judged to be of less practical importance. With regard to the present problem, the observed transport in the counterflow is at most a small fraction of the Gulf Stream transport.

One thus expects a nonlinear flow field as sketched in Fig. 9. Because of the finite topographic slope, the jet is confined to an inertial boundary layer next to the jet axis. Within this boundary layer, the vortex stretching as the jet enters the deeper water is balanced by a flow convergence toward the maximum cyclonic shear (the dashed line) and where an inner viscous boundary layer is confined. The entrainment of the inshore water by the jet induces a weak counterflow in the interior.

It is evident from above analyses that we have only derived a necessary condition for an inertial jet; namely, it must entrain the inshore water and induce a counterflow, but unlike the linear solution, we have not established the existence of such a flow. Indeed, compounded further by possible numerical instabilities, I have not yet obtained a numerical solution for the strongly nonlinear regime. But as we shall see next, the asymptotic analysis presented here nevertheless helps us to understand the modification of the linear balance when nonlinear terms are included.

c. *Applications*

A numerical solution using the parameter values of the large-scale case of MAB (section 3.4) and the same topography as in Fig. 8 is plotted in Fig. 10. Since $\epsilon = E^{1/3}$, the flow is not strongly nonlinear as depicted in Fig. 9; the balance of terms nevertheless shows the displacement of the viscous boundary layer to the cyclonic side of the jet, consistent with the asymptotic analysis. While the model flow is similar in appearance to the linear flow shown in Fig. 8, one should be aware of the significant difference in the underlying vorticity balance.

Although the similarity solution has required a specific boundary shape of $a = 1/3$, the fact that the jet is confined offshore suggests that the gross flow structure as shown in Fig. 10 is not overly sensitive to the boundary shape and should persevere in less idealized situations. One concludes then the variable-depth flow differs qualitatively from the constant-depth flow shown in Fig. 3, as has been suspected. Instead of a jet extending to the coastal boundary, there is a broad and weak counterflow inshore of the jet, which compares more favorably with the observed slope sea gyre. In addition, the predicted flow convergence toward the inshore edge of the jet is consistent with observed occurrence of the shelf water there and the inferred shoreward flux of nutrients across the jet axis (Csanady and Hamilton 1988).

5. Summary

To provide possible dynamical interpretations of the Gulf Stream induced circulation in the Middle Atlantic Bight (MAB), I have considered the inshore flow driven by a steady and straight jet in a homogeneous ocean. Similarity solutions are used to depict possible flow fields and the underlying dynamical balance.

To isolate the curvature effect of the coastal boundary, I have first considered the constant-depth ocean from which various nonlinear flow regimes are discerned, as illustrated in Fig. 2. Only with an accelerating jet (Regime I) can the strong flow extend to the coastal boundary where a viscous shear layer is confined. For a decelerating jet in a convergent geometry (Regime II), on the other hand, the viscous effect is expelled to the jet axis by an offshore flow, characterized by a large vorticity gradient. For a decelerating jet in a divergent geometry, the viscous effect remains important throughout the model domain by the generation of undulating flows. The counterflow immediately inshore of the jet is entrained into the jet when the coastal boundary is concave (Regime III) but is fed from the jet when the coastal boundary is convex (Regime IV). This last regime can explain the observed shoreward intrusion of the Gulf Stream water just downstream of Cape Hatteras.

Over the larger scale of the MAB, scale analysis suggests the importance of the topographic stretching in the vorticity balance. When the topography is incorporated, the similarity solution shows the jet to be confined offshore, flanked inshore by a weak counterflow, consistent with the observed slope sea gyre. In addition, there is a flow convergence toward the inshore edge of the jet, consistent with the observed occurrence of the shelf water there and the inferred shoreward flux of nutrients across the jet axis.

Acknowledgments. The work is supported by the Department of Energy under Grant DE-FG02-89ER60818 and the Office of Naval Research under Grant N00014-91-J-4053.

APPENDIX

The Numerical Method for Solving Eqs. (4.7) and (4.9)

Because of the presence of a regular singular point at the coastal boundary in the variable-depth model, we adopt a procedure of forward shooting. Namely, we guess the two unknown conditions at $\eta = 0$ and then integrate the equation forward to $\eta = 1$, upon which we check the other required boundary conditions, and the process is repeated until these boundary conditions are satisfied to the desired accuracy.

One may visualize a two-dimensional plane spanned by the axes representing the two unknown conditions at $\eta = 0$, that is, the values of $\phi(0)$ and $(\phi'/D)''(0)$, and two curves on this plane representing the required boundary conditions at $\eta = 1$, that is, $\phi(1) = 0$ and $(\phi'/D)(1) = 0$; the task is then to determine the intersect of these two curves. The procedure can be automated by first choosing an initial domain large enough to encompass the intersect and then systematically halving its linear dimension until the desired accuracy is achieved. For all the numerical solutions presented in this paper, a fourth-order Runge–Kutta scheme is used for integration, the grid spacing is 0.05, and the boundary conditions are satisfied to the third decimal place.

REFERENCES

Bane, J. M., Jr., O. B. Brown, R. H. Evans, and P. Hamilton, 1988: Gulf Stream remote forcing of shelfbreak currents in the Mid-Atlantic Bight. *Geophys. Res. Lett.*, **15**(5), 405–407.

Batchelor, G. K., 1970: *An Introduction to Fluid Dynamics.* Cambridge University Press, 615 pp.

Churchill, J. H., and P. C. Cornillon, 1991a: Water discharged from the Gulf Stream north of Cape Hatteras. *J. Geophys. Res.*, **96.**

——, and ——, 1991b: Gulf Stream water on the shelf and upper slope north of Cape Hatteras. *Contin. Shelf Res.*, **11,** 409–431.

——, ——, and P. Hamilton, 1989: Velocity and hydrographic structure of subsurface shelf water at the Gulf Stream's edge. *J. Geophys. Res.*, **94,** 10 791–10 800.

Csanady, G. T., and P. Hamilton, 1988: Circulation of slopewater. *Contin. Shelf Res.*, **8,** 565–624.

Ford, W. L., and A. R. Miller, 1952: The surface layer of the Gulf Stream and adjacent waters. *J. Mar. Res.*, **11,** 267–280.

Halliwell, G. R., Jr., and C. N. K. Mooers, 1979: The space-time structure and variability of the shelf water-slope water and Gulf Stream water fronts and associated warm-core eddies. *J. Geophys. Res.*, **84,** 7707–7722.

Rossby, C.-G., 1936: Dynamics of steady ocean currents in the light of experimental fluid mechanics. *Pap. Phys. Oceanogr. Meteor.*, **5**(1), 43 pp. [published by M.I.T. and W.H.O.I.]

Watts, D. R., 1983: Gulf Stream variability. *Eddies in Marine Science,* A. R. Robinson, Ed., Springer-Verlag, 609 pp.